

# Radiation Reaction Enhancement in Flying Focus Pulses

M. Formanek,<sup>1,\*</sup> D. Ramsey,<sup>2</sup> J. Palastro,<sup>2</sup> and A. Di Piazza<sup>1,†</sup>

<sup>1</sup>*Max Planck Institute for Nuclear Physics, Saupfercheckweg 1, D-69117 Heidelberg, Germany*

<sup>2</sup>*University of Rochester, Laboratory for Laser Energetics, Rochester, New York, 14623 USA*

Radiation reaction is the oldest still-unsolved problem in electrodynamics. In addition to conceptual difficulties in its theoretical formulation, the requirement of exceedingly large charge accelerations has thus far prevented its unambiguous experimental identification. Here, we show how radiation-reaction effects in a laser-electron interaction can be enhanced by orders of magnitude through the use of flying focus pulses (FFPs). By allowing the focus to counterpropagate with respect to the pulse phase velocity, a FFP overcomes the intrinsic limitation of a conventional laser Gaussian pulse (GP) that limits its focus to a Rayleigh range. For an electron initially also counterpropagating with respect to the pulse phase velocity, an extended interaction length with the laser peak intensity is achieved, which results in an overall deceleration far exceeding that in a GP with the same total energy and power. Using the Landau-Lifshitz equation of motion, we show numerically and analytically that the capability of emerging laser systems to deliver focused FFPs will allow for a clear experimental identification of radiation reaction.

Radiation reaction, i.e., the energy and momentum loss of an accelerated charge as it emits radiation, remains an outstanding issue in the formulation of classical electrodynamics [1–3]. The classical equation of motion accounting for radiation reaction, the Lorentz-Abraham-Dirac equation [4], suffers from causality issues, runaway solutions, and/or problems with initial conditions. To this day, radiation reaction remains an active area of research highlighted by a number of research [5–20] and review articles published over the last decade [21–25], as well as in recent experimental efforts to measure the effects of radiation reaction on electrons interacting with aligned crystals [26, 27] and ultrastrong laser fields [28, 29]. Apart from its fundamental importance, relating, e.g., to intrinsic properties of elementary particles like the mass of the electron, RR plays a crucial role in several fields of physics, such as astrophysics, plasma, and accelerator physics.

Flying focus is a newly developed technique for controlling the trajectory of peak laser intensity over distances much longer than the Rayleigh range [30, 31]. In the original experimental demonstrations, the peak intensity was made to travel at any desired velocity by adjusting the chirp and using a chromatic lens to independently set the time and location at which each frequency within the pulse came to focus [30, 31]. More recent implementations have proposed axiparabola-echelon optics [32] and ‘space-time light sheets’ [33, 34] to achieve the same effect. Building on this capability, several studies have illustrated the advantage of flying focus pulses (FFPs) for a wide range of laser-based applications, including ionization waves [35, 36], photon acceleration [37], laser wakefield acceleration [32], vacuum electron acceleration [38], and nonlinear Thomson scattering [39].

In the present Letter we show that FFPs can increase radiation reaction deceleration of electrons (charge  $e < 0$  and mass  $m$ ) by orders of magnitude when compared to Gaussian pulses (GPs) with the same energy and

power/peak intensity. The high-intensity region of a GP is set to the Rayleigh range which defines a limited spatial domain through which an ultrarelativistic electron quickly passes. In contrast, the peak intensity of a FFP can move at the speed of light and in the opposite direction of its laser phase velocity (Fig. 1). Thus, an ultrarelativistic electron traveling in the opposite direction of the phase fronts can remain in the ‘focus’ of a FFP for extended interaction times limited only by the total pulse energy. In order to clearly compare the performances of both field configurations, we first analytically calculate the electron energy loss starting from the relativistic Larmor formula. Then, we validate these results numerically by simulating the electron trajectories using the Landau-Lifshitz equation for radiation reaction. The orders of magnitude amplification of radiation-reaction effects enabled by FFPs provide a unique tool to unambiguously identify this elusive phenomenon in experiments.

It was shown in Ref. [40] that the exact solution of Maxwell’s equations given in Ref. [41] describes a flying focus beam (FFB) with a fixed focal velocity  $v_f = -1$  equal and opposite to the direction of the phase velocity (units with  $\hbar = c = \epsilon_0 = 1$  are used throughout). Here, we employ this solution to model the FFBs because (i) it satisfies the vacuum wave equation exactly; (ii) the electric and magnetic fields can be expressed analytically in closed form; (iii) its exponential drop-off in the transverse direction assures a finite beam power, which is important for a direct comparison with Gaussian beams (GBs). We indicate as  $A^\mu(x)$  the four-vector potential of the FFB and we work within the Lorenz gauge  $\partial \cdot A = 0$ , with the additional condition  $A_+(x) = A^0(x) + A^z(x) = 0$  [40]. For the sake of completeness, we report the expression of the four-vector potential, which is an exact solution of the vacuum wave equation  $\partial^2 A^\mu = 0$ , in the case of a monochromatic spectral profile (see Ref. [40] for the case of the Gaussian spectral profile and the Supplemental Material (SM) [42] also for the case of beams featuring

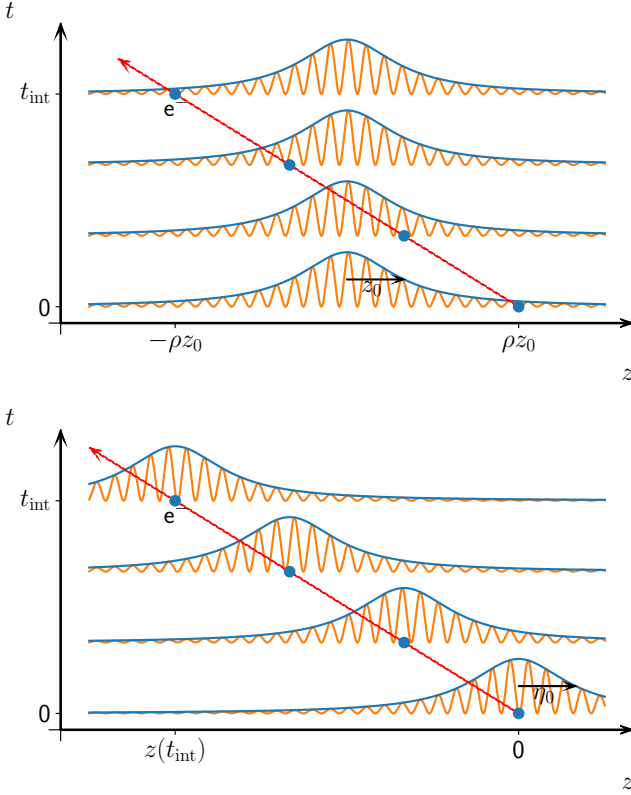


FIG. 1. Schematic representation of an ultrarelativistic electron counterpropagating with respect to a stationary Gaussian beam (top panel) and to a flying focus beam with focal velocity equal and opposite to the phase velocity (bottom panel). For the sake of clarity the laser-pulse envelope is not included here (see the text for details). The axes are not to scale.

a non-zero angular momentum). For a FFB polarized along the  $x$ -axis with a wave-vector pointing in the direction of the positive  $z$ -axis, the non-zero four-potential components are

$$A^x = \mathcal{A}_0 \frac{\sigma_0}{\sigma_\eta} e^{-r^2/\sigma_\eta^2} \cos[\Psi(0)], \quad (1a)$$

$$A^0 = -A^z = \frac{\mathcal{A}_0}{\omega_0} \frac{x}{\sigma_\eta^2} e^{-r^2/\sigma_\eta^2} \sin[\Psi(1)]. \quad (1b)$$

Here, we have introduced the four-potential amplitude  $\mathcal{A}_0$ , the spot radius  $\sigma_0$ , and the angular frequency  $\omega_0 = 2\pi/\lambda_0$  as the main quantities characterizing the beam. Also, we employ light-cone coordinates  $\phi = t - z$ ,  $\eta = t + z$ , and  $\mathbf{r} = (x, y)$ , such that  $r = \sqrt{x^2 + y^2}$  is the distance from the  $z$ -axis, and

$$\sigma_\eta = \sigma_0 \sqrt{1 + \eta^2/\eta_0^2}, \quad \eta_0 = \omega_0 \sigma_0^2, \quad (2)$$

which implies that the focus of the FFB is placed at  $\eta = t + z = 0$ , i.e., that the focal velocity is  $-1$ . Finally, the

phase  $\Psi(a)$  is defined as

$$\Psi(a) = \omega_0 \phi - \frac{r^2}{\sigma_\eta^2} \frac{\eta}{\eta_0} + (1 + a) \arctan\left(\frac{\eta}{\eta_0}\right). \quad (3)$$

For the GBs we employ the solution within the paraxial approximation in which the diffraction angle  $\theta = \sigma_0/z_0$  is the small parameter [43]. Here,  $\sigma_0$  is the spot radius and  $z_0 = \omega_0 \sigma_0^2/2$  is the Rayleigh length such that  $\theta \approx 0.3$  for a beam focused down to a single wavelength. We again consider a linearly polarized field in the  $x$ -direction with the wave vector pointing along the positive  $z$ -axis. The solution of the paraxial equation satisfying the Lorenz gauge condition  $\partial \cdot A = 0$  and  $A^z = 0$  is given by

$$A^x = \mathcal{A}_0 \frac{\sigma_0}{\sigma_z} e^{-r^2/\sigma_z^2} \cos[\Phi(0)], \quad (4a)$$

$$A^0 = \frac{\mathcal{A}_0}{\omega_0} \frac{2x}{\sigma_z^2} e^{-r^2/\sigma_z^2} \sin[\Phi(1)], \quad (4b)$$

where

$$\sigma_z = \sigma_0 \sqrt{1 + z^2/z_0^2}, \quad (5)$$

which places the focus of the GB at  $z = 0$ , and

$$\Phi(a) = \omega_0 \phi - \frac{r^2}{\sigma_z^2} \frac{z}{z_0} + (1 + a) \arctan\left(\frac{z}{z_0}\right). \quad (6)$$

We emphasize that the main mathematical and conceptual difference between the FFB and GB is that in order to describe the FFB we replace the  $z$ -dependent  $\sigma_z$  (5) by the  $\eta$ -dependent  $\sigma_\eta$  (2). Thus, we conclude that, unlike in GBs where the focus is fixed in space, it moves in the FFB at the speed of light in negative  $z$ -direction (recall that  $\eta = t + z$ ), i.e., opposite to the propagation direction of the phase fronts.

The time-averaged power of the GB going through the transversal  $xy$ -plane can be expressed in the paraxial approximation as [44]

$$P_{\text{ave}} = \frac{\pi}{4} \mathcal{A}_0^2 \omega_0^2 \sigma_0^2 \approx 21.5 [\text{GW}] \left( \xi_0 \frac{\sigma_0}{\lambda_0} \right)^2, \quad (7)$$

where  $\xi_0 = |e| \mathcal{A}_0/m$  is the dimensionless normalized amplitude, which is related to the laser peak intensity  $I_0$  as  $I_0 [\text{W/cm}^2] = 1.37 \times 10^{18} \xi_0^2 (\lambda_0 [\mu\text{m}])^{-2}$ . The corresponding expression for the FFB is the same (see the SM [42]). Both these expressions are derived under the assumption that the field oscillations are faster than the rate of change of the envelope, i.e., that the Rayleigh length is much larger than the laser wavelength:  $\sigma_0^2 \geq \lambda_0^2/\pi$ .

In order to model pulses of finite energy, we employ a slowly-varying envelope  $g(\phi)$  with a constant flattop profile moving at the speed of light against the motion of the electron. The analytical flying focus solution also allows us to implement this exactly without violating the

Maxwell equations, by utilizing a finite spread in the frequency domain (see Ref. [40] and the SM [42]). Because modeling specific pulse profiles requires performing non-analytical Fourier transformations, we work in an approximation of long pulses and neglect any derivatives of the envelope  $g(\phi)$ . For a total pulse energy  $E_{\text{tot}}$  and average power  $P_{\text{ave}}$ , the pulse length is given by  $\tau = E_{\text{tot}}/P_{\text{ave}}$ . If spatial focusing effects are ignored, i.e., for a plane wave characterized by the envelope  $g(\phi)$ , and if a pulse counterpropagating with respect to an ultrarelativistic electron is considered, then the wave-electron interaction time  $t_{\text{int}}$  is approximately given by  $\tau/2$ .

Since we are going to consider ultrarelativistic electrons at the focus of the laser field, for the sake of analytical estimations, we will assume that the latter can be locally approximated as a plane wave with the dimensionless amplitude  $\xi(t)$  given by the field value at  $r = 0$ . Also, in the ultrarelativistic limit the electron energy loss can be directly computed from the relativistic Larmor formula  $P_L = -m\tau_0\dot{u}^2$  of the electromagnetic radiated power [we use the diagonal metric tensor  $(+1, -1, -1, -1)$ ]. Here, the characteristic time  $\tau_0 = e^2/(6\pi m) = 6.26 \times 10^{-24}$  s and the proper-time derivative  $\dot{u}^\mu$  of the four-velocity  $u^\mu = \gamma(1, \boldsymbol{\beta})$  have been introduced. This corresponds to the energy loss  $d\gamma/dt = \tau_0\dot{u}^2$ , where  $\dot{u}^2 = -\xi^2(t)(k_0 \cdot u)^2$  in a plane-wave with four-wave-vector  $k_0^\mu = (\omega_0, \mathbf{k}_0)$ . For a ultrarelativistic electron moving in the direction opposite the wave vector  $\mathbf{k}_0$ , the invariant product  $k_0 \cdot u$  is approximately  $2\omega_0\gamma$  and correspondingly the variable  $\phi$  along the electron trajectory is approximately  $2t$ . Thus, the differential equation for the electron gamma factor  $\gamma(t)$  with the initial condition  $\gamma(0) = \gamma_0$  has the approximate solution [45]

$$\gamma(t) \approx \frac{\gamma_0}{1 + 2\gamma_0\tau_0\omega_0^2 \int_0^t \xi^2(t')dt'} = \frac{\gamma_0}{1 + \kappa(t)}, \quad (8)$$

where  $\kappa(t) = 2\gamma_0\tau_0\omega_0^2 \int_0^t \xi^2(t')dt'$  represents the deceleration factor after a time  $t$  and where the integral is taken over the slowly-varying amplitude function  $\xi(t)$  to be computed along the electron trajectory at  $r = 0$ .

In the case of the GP the amplitude changes as  $\xi(t) = \xi_0/\sqrt{1 + z^2(t)/z_0^2}$ . We assume the best-case scenario where the electron interacts with the pulse while moving through the region of its highest focus. Thus, the electron trajectory is approximately given by  $r(t) = 0$  and  $z(t) = \rho z_0 - t$ , where  $r(0) = 0$  and  $z(0) = \rho z_0$  is the initial electron position, with  $\rho$  being a dimensionless parameter defined according to the following considerations. We set the ‘‘final’’ electron position at  $t = t_{\text{int}}$ , i.e., after moving through the whole focal region at almost the speed of light, to the value  $z(t_{\text{int}}) = -\rho z_0$  (see the top panel of Fig. 1). Thus  $t_{\text{int}} = 2\rho z_0$ , and the parameter  $\rho$  gives half of the number of Rayleigh lengths  $z_0$  over which the electron interacts with a GP

with fixed total pulse energy  $E_{\text{tot}}$  and average power  $P_{\text{ave}}$ :  $\rho = E_{\text{tot}}/(4z_0P_{\text{ave}})$ . The integral in Eq. (8) can be evaluated as  $\int_0^{t_{\text{int}}} \xi^2(t')dt' = 2\xi_0^2 z_0 \arctan(\rho)$ . By using for the average power  $P_{\text{ave}}$  the power formula in Eq. (7), the deceleration factor  $\kappa_{\text{GP}}$  after the interaction time  $t_{\text{int}}$  can be expressed as

$$\begin{aligned} \kappa_{\text{GP}}(t_{\text{int}}) &= \frac{32}{3} \frac{E_{\text{tot}}\mathcal{E}_0}{m^2} \left(\frac{r_e}{\sigma_0}\right)^2 \frac{\arctan(\rho)}{\rho} \\ &\approx 2.03 \frac{E_{\text{tot}}[\text{J}]}{\sigma_0^2[\mu\text{m}]} \frac{\mathcal{E}_0[\text{GeV}]}{\rho} \arctan(\rho), \end{aligned} \quad (9)$$

where  $\mathcal{E}_0 = m\gamma_0$  is the initial electron energy and  $r_e = e^2/(4\pi m)$  is the classical electron radius. This means that at fixed pulse energy  $E_{\text{tot}}$  the deceleration factor is larger for smaller focal spot sizes  $\sigma_0 \rightarrow 0$  and smaller interaction times  $\rho \rightarrow 0$ . Both these trends require increasing the beam amplitude and beam power to keep the total pulse energy  $E_{\text{tot}}$  fixed. This can be seen from the relation  $P_{\text{ave}} = E_{\text{tot}}/2t_{\text{int}} \sim E_{\text{tot}}/\sigma_0^2\rho$  and, taking into account Eq. (7),  $\xi_0^2 \sim P_{\text{ave}}/\sigma_0^2 \sim E_{\text{tot}}/\sigma_0^4\rho$ .

In principle, the deceleration factor can be arbitrarily large (until the electron stops) but, as we decrease  $\sigma_0$  and  $\rho$ , we run into issues with the paraxial approximation, with the assumptions for deriving the beam power formula (7) and the deceleration formula (8), not to mention the difficulties in the experimental feasibility of such pulses. Therefore, we limit the GPs to a certain fixed power  $P_{\text{fix}}$  or fixed amplitude  $\xi_{\text{fix}}$ . In these cases the interaction parameter  $\rho$  is given respectively by

$$\rho(P_{\text{fix}}) = \frac{1}{2\omega_0\sigma_0^2} \frac{E_{\text{tot}}}{P_{\text{fix}}} \approx \frac{2.4 \times 10^{-2} E_{\text{tot}}[\text{J}]\lambda_0[\mu\text{m}]}{P_{\text{fix}}[\text{PW}]\sigma_0^2[\mu\text{m}]}, \quad (10)$$

$$\rho(\xi_{\text{fix}}) = \frac{8r_e}{\omega_0^3\sigma_0^4} \frac{E_{\text{tot}}}{m\xi_{\text{fix}}^2} \approx \frac{1.1 \times 10^3 E_{\text{tot}}[\text{J}]\lambda_0^3[\mu\text{m}]}{\xi_{\text{fix}}^2\sigma_0^4[\mu\text{m}]}. \quad (11)$$

The estimates for the deceleration factor  $\kappa$  are then obtained by substituting these expressions into Eq. (9).

For the FFP the situation is considerably simpler because the electron can co-travel with the moving focus for the duration of the interaction  $t_{\text{int}}$  (see bottom panel of Fig. 1). Then the integrand in Eq. (8) is constant and  $\int_0^{t_{\text{int}}} \xi^2(t')dt' = \xi_0^2 t_{\text{int}}$ . By using the expression of the power  $P_{\text{ave}} = E_{\text{tot}}/(2t_{\text{int}})$  and Eq. (7), we can again eliminate  $\xi_0^2$  and obtain the final deceleration factor at fixed total pulse energy

$$\begin{aligned} \kappa_{\text{FFP}}(t_{\text{int}}) &= \frac{32}{3} \frac{E_{\text{tot}}\mathcal{E}_0}{m^2} \left(\frac{r_e}{\sigma_0}\right)^2 \\ &\approx 2.03 \frac{E_{\text{tot}}[\text{J}]\mathcal{E}_0[\text{GeV}]}{\sigma_0^2[\mu\text{m}]}. \end{aligned} \quad (12)$$

We note that this result does not depend on  $P_{\text{ave}}$  or  $\xi_0$ . Thus, one can obtain the same deceleration effect by decreasing the average power, provided that the interaction time  $t_{\text{int}} = E_{\text{tot}}/2P_{\text{ave}}$  increases accordingly. An analogous consideration holds if one decides to decrease the

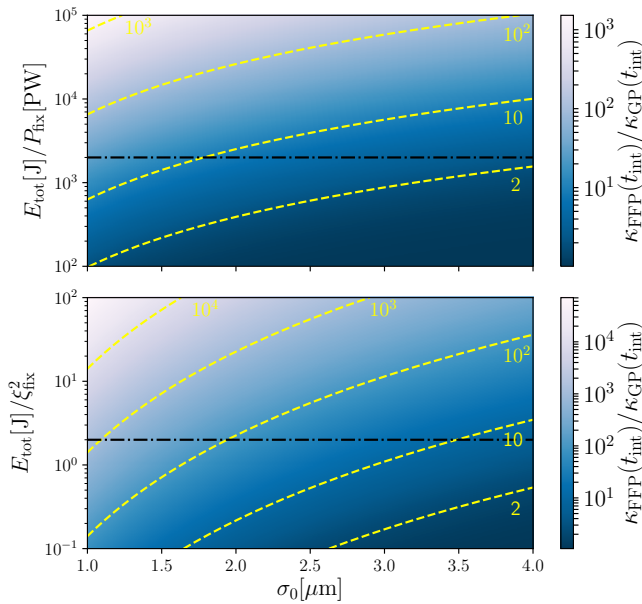


FIG. 2. The ratio  $\kappa_{\text{FFP}}(t_{\text{int}})/\kappa_{\text{GP}}(t_{\text{int}})$  as a function of the pulse parameters. The top panel shows the case when the average beam power is fixed, whereas the bottom panel shows the case where the laser amplitude is fixed. The laser wavelength is  $\lambda_0 = 1 \mu\text{m}$  in both cases. The dashed yellow lines correspond to  $\kappa_{\text{FFB}}(t_{\text{int}})/\kappa_{\text{GB}}(t_{\text{int}}) = 2$  and powers of ten, as indicated. The black dash-dotted lines correspond to the numerical cases from Fig. 3.

field amplitude  $\xi_0$ . In other words, FFPs allow us to decrease at will either the beam power or its amplitude in a trade-off for a longer interaction time. This is not possible for GPs whose interaction with charged particles is limited by the Rayleigh length [see Eq. (9)].

In order to show the advantage of using a FFP as compared to a GP based on the estimates above, we look at the ratio  $\kappa_{\text{FFP}}(t_{\text{int}})/\kappa_{\text{GP}}(t_{\text{int}}) = \rho/\arctan(\rho)$  for a given total pulse energy  $E_{\text{tot}}$  and initial electron energy  $\mathcal{E}_0$ . In Fig. 2 we plot this ratio as a function of the pulse parameters for either fixed power  $P_{\text{fix}}$  [top panel and  $\rho$  given by Eq. (10)] or fixed amplitude  $\xi_{\text{fix}}$  [bottom panel and  $\rho$  given by Eq. (11)]. We see that for a fixed total energy  $E_{\text{tot}}$  for smaller and smaller values of either  $P_{\text{fix}}$  or  $\xi_{\text{fix}}$ , the FFPs have a clear advantage over the GPs by more than one order of magnitude.

In order to demonstrate the enhancement of radiation-reaction deceleration in a FFP, we have numerically solved for the electron motion in GPs and FFPs using the Landau-Lifshitz equation [1]

$$\begin{aligned} \dot{u}^\mu &= \frac{e}{m} F^{\mu\nu} u_\nu \\ &+ \tau_0 \frac{e}{m} \left[ \frac{d}{d\tau} (F^{\mu\nu}) u_\nu + \frac{e}{m} P_\nu^\mu F^{\nu\alpha} F_{\alpha\beta} u^\beta \right], \end{aligned} \quad (13)$$

where  $P_\nu^\mu = \delta_\nu^\mu - u^\mu u_\nu$  is the projector orthogonal to

$u^\mu$  and  $F^{\mu\nu} = \partial^\mu A^\nu - \partial^\nu A^\mu$  the electromagnetic field tensor with four-potentials given by Eqs. (1a) and (1b) and by Eqs. (4a) and (4b) for the FFB and the GB, respectively. We have ensured numerically that the term proportional to the proper-time derivative of the field is negligible, see for example also Refs. [46, 47] and omitted it from simulations. The total pulse energy was set to  $E_{\text{tot}} = 200 \text{ J}$ , the initial electron gamma factor to  $\gamma_0 = 1000$  ( $\mathcal{E}_0 = 0.511 \text{ GeV}$ ), and the laser wavelength  $\lambda_0 = 1 \mu\text{m}$ . We investigated the case where the power is fixed to  $P_{\text{fix}} = 0.1 \text{ PW}$  (top panel of Fig. 3) and where the normalized dimensionless amplitude is fixed to  $\xi_{\text{fix}} = 10$  i.e.,  $I_0 = 1.37 \times 10^{20} \text{ W/cm}^2$  (bottom panel of Fig. 3). The laboratory time step was set to  $dt = 0.005 \text{ } 1/k_0$  or smaller. Also, the above mentioned envelope function  $g(\phi)$  was implemented, which introduces a smooth, symmetric, 5th order polynomial switch on/off for the fields and a constant flat profile for the duration of the interaction. See SM [42] for details.

Fig. 3 shows that for the GPs the energy loss estimates from Eq. (9) are in an excellent agreement with the numerical results. This is also the case for the FFPs with the exception of the most focused pulses when  $\sigma_0/\lambda_0 < 3$ . Once the electron is decelerated to  $\gamma \sim 30$  and lower, the interaction with the pulse becomes more complicated than our estimates capture. For example, the electrons begin to lag behind the FFP and experience additional ponderomotive deceleration [39]. Finally, if  $\xi_0$  is sufficiently large, the transverse oscillations become important and the electron can be ejected from the optical axis. Significant transverse oscillations also imply that the approximation  $k_0 \cdot u \approx 2\omega_0\gamma$  used for deriving Eq. (8) is no longer valid. For the numerical results with fixed power, the electron even came to a stop in the longitudinal direction and reversed its direction of motion for  $\sigma_0/\lambda_0 < 2$ . Thus the first five data points for FFPs in both panels of Fig. 3 were calculated from the minimum  $\gamma$  along the simulated electron trajectory.

Figures 2 and 3 clearly demonstrate the advantage of using FFPs as compared with GPs in order to enhance radiation reaction. Presently, measuring the electron energy seems to be the most direct way of detecting radiation-reaction effects [28, 29]. In focused FFPs, with accessible laser powers and peak intensities, it is possible to strip ultrarelativistic electrons of a substantial fraction of their energy, which is expected to be readily measurable experimentally.

In conclusion, we have shown that FFPs provide an orders-of-magnitude enhancement of radiation-reaction effects as compared to conventional GPs of the same energy and power/peak intensity. This large enhancement was achieved by exploiting the cumulative nature of radiation-reaction effects and the unique properties of the FFPs, for which the peak intensity can move in the opposite direction of the phase velocity. The FFP advantage becomes more pronounced as the spot size de-

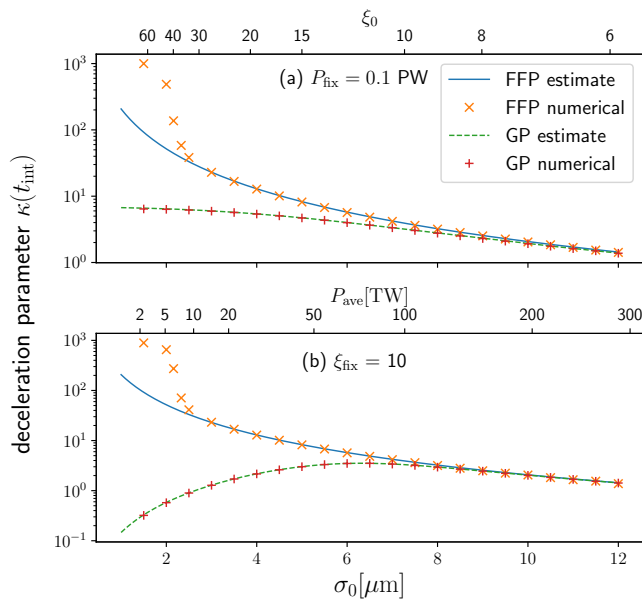


FIG. 3. Comparison of the radiation reaction deceleration  $\kappa(t_{\text{int}})$  of an electron with  $E_0 = 0.511$  GeV in the FFP and GP. The laser wavelength is  $\lambda_0 = 1 \mu\text{m}$ . For the first five data points the maximal  $\kappa$  along the electron trajectory is plotted. The pulses are kept at fixed energy  $E_{\text{tot}} = 200$  J and either fixed power  $P_{\text{fix}} = 0.1$  PW (part (a)) or fixed amplitude  $\xi_{\text{fix}} = 10$ , corresponding to  $I_0 = 1.37 \times 10^{20} \text{W}/\text{cm}^2$  (part (b)). The curves are analytical estimates and the points result from the numerical simulations. The upper  $x$ -axes show the dimensionless amplitude for the fixed-power case in part (a) and the laser power for the fixed amplitude case in part (b).

creases, and currently  $\sigma_0 \approx 3\lambda_0$  is within experimental reach. Thus, our present results also motivate the experimental implementation of FFPs in applications aiming at measuring the dynamics driven by radiation reaction.

We would like to thank Dustin Froula, Warren Mori, Jorge Vieira, and Marija Vranic for useful discussions. This material is also based upon work supported by the Office of Fusion Energy Sciences under Award Number DE-SC0019135 and DE-SC00215057, the Department of Energy National Nuclear Security Administration under Award Number DE-NA0003856, the University of Rochester, and the New York State Energy Research and Development Authority.

\* formanek@mpi-hd.mpg.de

† dipiazza@mpi-hd.mpg.de

- [1] L. D. Landau and E. M. Lifshitz, *The Classical Theory of Fields* (Elsevier, Oxford, 1975).
- [2] A. O. Barut, *Electrodynamics and Classical Theory of Fields and Particles* (Dover, New York, 1980).
- [3] F. Rohrlich, *Classical Charged Particles* (World Scien-

tific, Singapore, 2007).

- [4] P. A. M. Dirac, Proc. R. Soc. London, Ser. A **167**, 148 (1938).
- [5] M. Vranic, J. L. Martins, J. Vieira, R. A. Fonseca, and L. O. Silva, Phys. Rev. Lett. **113**, 134801 (2014).
- [6] T. G. Blackburn, C. P. Ridgers, J. G. Kirk, and A. R. Bell, Phys. Rev. Lett. **112**, 015001 (2014).
- [7] M. Tamburini, C. H. Keitel, and A. Di Piazza, Phys. Rev. E **89**, 021201(R) (2014).
- [8] J.-X. Li, K. Z. Hatsagortsyan, and C. H. Keitel, Phys. Rev. Lett. **113**, 044801 (2014).
- [9] T. Heinzl, C. Harvey, A. Ilderton, M. Marklund, S. S. Bulanov, S. Rykovanov, C. B. Schroeder, E. Esarey, and W. P. Leemans, Phys. Rev. E **91**, 023207 (2015).
- [10] S. R. Yoffe, Y. Kravets, A. Noble, and D. A. Jaroszynski, New J. Phys. **17**, 053025 (2015).
- [11] R. Capdessus and P. McKenna, Phys. Rev. E **91**, 053105 (2015).
- [12] M. Vranic, T. Grismayer, R. A. Fonseca, and L. O. Silva, New J. Phys. **18**, 073035 (2016).
- [13] V. Dinu, C. Harvey, A. Ilderton, M. Marklund, and G. Torgrimsson, Phys. Rev. Lett. **116**, 044801 (2016).
- [14] A. Di Piazza, T. N. Wistisen, and U. I. Uggerhøj, Phys. Lett. B **765**, 1 (2017).
- [15] C. N. Harvey, A. Gonoskov, A. Ilderton, and M. Marklund, Phys. Rev. Lett. **118**, 105004 (2017).
- [16] C. P. Ridgers, T. G. Blackburn, D. Del Sorbo, L. E. Bradley, C. Slade-Lowther, C. D. Baird, S. P. D. Mangles, P. McKenna, M. Marklund, C. D. Murphy, and A. G. R. Thomas, J. Plasma Phys. **83**, 715830502 (2017).
- [17] F. Niel, C. Riconda, F. Amiranoff, R. Ducloux, and M. Grech, Phys. Rev. E **97**, 043209 (2018).
- [18] F. Niel, C. Riconda, F. Amiranoff, M. Lobet, J. Derouillat, F. Pérez, T. Vinci, and M. Grech, Plasma Phys. Controlled Fusion **60**, 094002 (2018).
- [19] M. Formanek, A. Steinmetz, and J. Rafelski, Physical Review D **102**, 056015 (2020).
- [20] A. Di Piazza and G. Audagnotto, Phys. Rev. D **104**, 016007 (2021).
- [21] R. T. Hammond, Electron. J. Theor. Phys. **7**, 221 (2010).
- [22] A. Di Piazza, C. Müller, K. Z. Hatsagortsyan, and C. H. Keitel, Rev. Mod. Phys. **84**, 1177 (2012).
- [23] D. A. Burton and A. Noble, Contemp. Phys. **55**, 110 (2014).
- [24] T. G. Blackburn, Rev. Mod. Plasma Phys. **4**, 5 (2020).
- [25] A. Gonoskov, T. Blackburn, M. Marklund, and S. Bulanov, preprint arXiv:2107.02161 (2021).
- [26] T. N. Wistisen, A. Di Piazza, H. V. Knudsen, and U. I. Uggerhøj, Nat. Commun. **9**, 795 (2018).
- [27] C. F. Nielsen, J. B. Justesen, A. H. Sorensen, U. I. Uggerhøj, and R. Holtzapple, New Journal of Physics (2021).
- [28] J. M. Cole, K. T. Behm, E. Gerstmayr, T. G. Blackburn, J. C. Wood, C. D. Baird, M. J. Duff, C. Harvey, A. Ilderton, A. S. Joglekar, K. Krushelnick, S. Kuschel, M. Marklund, P. McKenna, C. D. Murphy, K. Poder, C. P. Ridgers, G. M. Samarin, G. Sarri, D. R. Symes, A. G. R. Thomas, J. Warwick, M. Zepf, Z. Najmudin, and S. P. D. Mangles, Phys. Rev. X **8**, 011020 (2018).
- [29] K. Poder, M. Tamburini, G. Sarri, A. Di Piazza, S. Kuschel, C. D. Baird, K. Behm, S. Bohlen, J. M. Cole, D. J. Corvan, M. Duff, E. Gerstmayr, C. H. Keitel, K. Krushelnick, S. P. D. Mangles, P. McKenna, C. D. Murphy, Z. Najmudin, C. P. Ridgers, G. M. Samarin, D. R. Symes, A. G. R. Thomas, J. Warwick, and M. Zepf,

- Phys. Rev. X **8**, 031004 (2018).
- [30] A. Sainte-Marie, O. Gobert, and F. Quéré, *Optica* **4**, 1298 (2017).
  - [31] D. H. Froula, D. Turnbull, A. S. Davies, T. J. Kessler, D. Haberberger, J. P. Palastro, S.-W. Bahk, I. A. Begishev, R. Boni, S. Bucht, J. Katz, and J. L. Shaw, *Nat. Photonics* **12**, 262 (2018).
  - [32] J. P. Palastro, J. L. Shaw, P. Franke, D. Ramsey, T. T. Simpson, and D. H. Froula, *Phys. Rev. Lett.* **124**, 134802 (2020).
  - [33] H. E. Kondakci and A. F. Abouraddy, *Nature Photonics* **11**, 733 (2017).
  - [34] M. Yessenov and A. F. Abouraddy, *Phys. Rev. Lett.* **125**, 233901 (2020).
  - [35] D. Turnbull, P. Franke, J. Katz, J. P. Palastro, I. A. Begishev, R. Boni, J. Bromage, A. L. Milder, J. L. Shaw, and D. H. Froula, *Phys. Rev. Lett.* **120**, 225001 (2018).
  - [36] J. P. Palastro, D. Turnbull, S.-W. Bahk, R. K. Follett, J. L. Shaw, D. Haberberger, J. Bromage, and D. H. Froula, *Phys. Rev. A* **97**, 033835 (2018).
  - [37] A. J. Howard, D. Turnbull, A. S. Davies, P. Franke, D. H. Froula, and J. P. Palastro, *Phys. Rev. Lett.* **123**, 124801 (2019).
  - [38] D. Ramsey, P. Franke, T. Simpson, D. Froula, and J. Palastro, *Physical Review E* **102**, 043207 (2020).
  - [39] D. Ramsey, B. Malaca, A. Di Piazza, M. Formanek, P. Franke, D. H. Froula, T. T. Simpson, J. Vieira, K. Weichman, and J. P. Palastro, preprint arXiv:2108.04044 (2021).
  - [40] A. Di Piazza, *Phys. Rev. A* **103**, 012215 (2021).
  - [41] E. Esarey, P. Sprangle, M. Pilloff, and J. Krall, *J. Opt. Soc. Am. B* **12**, 1695 (1995).
  - [42] See Supplemental Material at [URL will be inserted by publisher] for details about derivation of flying focus fields (also with non-zero angular momentum) and their properties.
  - [43] Y. I. Salamin, *Appl. Phys. B* **86**, 319 (2007).
  - [44] E. Esarey, S. K. Ride, and P. Sprangle, *Phys. Rev. E* **48**, 3003 (1993).
  - [45] A. Di Piazza, *Lett. Math. Phys.* **83**, 305 (2008).
  - [46] M. Tamburini, F. Pegoraro, A. Di Piazza, C. H. Keitel, and A. Macchi, *New J. Phys.* **12**, 123005 (2010).
  - [47] F. Li, V. K. Decyk, K. G. Miller, A. Tableman, F. S. Tsung, M. Vranic, R. A. Fonseca, and W. B. Mori, *Journal of Computational Physics* **438**, 110367 (2021).

# Supplemental Material: Radiation Reaction Enhancement in Flying Focus Pulses

M. Formanek,<sup>1</sup> D. Ramsey,<sup>2</sup> J. Palastro,<sup>2</sup> and A. Di Piazza<sup>1</sup>

<sup>1</sup>*Max Planck Institute for Nuclear Physics, Saupfercheckweg 1, D-69117 Heidelberg, Germany*

<sup>2</sup>*University of Rochester, Laboratory for Laser Energetics, Rochester, New York, 14623 USA*

The purpose of this supplemental document is to introduce the flying focus fields used in the associated Letter and their properties. We show how to construct flying focus beams and pulses as an exact solution of Maxwell's equations with arbitrary orbital angular momentum  $\ell$ . Then, we explicitly evaluate the electric and magnetic fields for the case  $\ell = 0$  and construct their field invariants. We also present a method of computing the power in the beam going through a transversal plane under the assumption that the phase oscillations of the fields are faster than the rate of change of the intensity envelope along the longitudinal direction. Finally, we describe our implementation of the pulse envelope.

## FLYING FOCUS BEAMS AND PULSES

We follow the solution method of Maxwell's equations presented in Ref. [1], which was shown to describe flying focus beams only recently [2], for the case of the focus moving at the speed of light in the opposite direction of the wave fronts. Here, we extend the solution to arbitrary angular momenta of the beam. We define light-cone coordinates  $\phi = t - z$ ,  $\eta = t + z$  for a wave whose wave fronts move at the speed of light in the direction of the positive  $z$ -axis (we work in units  $\hbar = c = \varepsilon_0 = 1$ ). In terms of these coordinates, we can write the electromagnetic field four-potential  $A^\mu$  in general as

$$A^\mu(\eta, \mathbf{r}, \phi) = \frac{1}{2} \int d\omega \tilde{A}^\mu(\eta, \mathbf{r}, \omega) e^{-i\omega\phi} + \text{c.c.}, \quad (1)$$

which is a Fourier transformation in the variables  $\omega \rightarrow \phi$ , and  $\mathbf{r} = (x, y)$  are the transverse coordinates.

The four-potential components  $A_-$  and  $A_+$  are defined as  $A_- = A^0 - A^z$ ,  $A_+ = A^0 + A^z$ . Thus, the Lorenz gauge condition  $\partial \cdot A = 0$  in the light-cone coordinates becomes

$$\partial_\phi A_- + \nabla_\perp \cdot \mathbf{A}_\perp + \partial_\eta A_+ = 0, \quad (2)$$

where  $\partial_\phi = (\partial_0 - \nabla_z)/2$  and  $\partial_\eta = (\partial_0 + \nabla_z)/2$ . We can set  $A_+ = 0$  as additional condition to leave us with two degrees of freedom of the electromagnetic field. By substituting Eq. (1) into Eq. (2), we obtain for the components of  $\tilde{A}^\mu$  the relationship

$$\tilde{A}_- = -\frac{i}{\omega} \nabla_\perp \cdot \tilde{\mathbf{A}}_\perp. \quad (3)$$

The wave equation  $\partial^2 A^\mu = 0$  in light-cone coordinates reads

$$(4\partial_\phi\partial_\eta - \nabla_\perp^2)A^\mu = 0, \quad (4)$$

which gives us in the frequency domain for the  $\tilde{\mathbf{A}}_\perp$  components the equation

$$-4i\omega\partial_\eta\tilde{\mathbf{A}}_\perp - \nabla_\perp^2\tilde{\mathbf{A}}_\perp = 0. \quad (5)$$

This differential equation has exactly the same form of the paraxial equation for the Gaussian beams differing only by a factor of two in the first term. Thus, any solution of this type of equation in the context of Gaussian beams within the paraxial approximation represents here an exact solution of Maxwell's equations in light-cone coordinates. In cylindrical coordinates  $(r, \theta, \eta)$ , with  $r = \sqrt{x^2 + y^2}$  being the distance from the  $z$ -axis, we can write

$$\left( \partial_r^2 + \frac{1}{r}\partial_r + \frac{1}{r^2}\partial_\theta^2 + 4i\omega\partial_\eta \right) \tilde{\mathbf{A}}_\perp = 0, \quad (6)$$

which has the analytical solution [3]

$$\begin{aligned} \tilde{\mathbf{A}}_{n,\ell,\perp}(\eta, r, \theta, \omega) &= \mathcal{A}_0 f(\omega) \frac{\sigma_0}{\sigma(\eta, \omega)} \left[ \frac{\sqrt{2}r}{\sigma(\eta, \omega)} \right]^\ell L_n^\ell \left[ \frac{2r^2}{\sigma^2(\eta, \omega)} \right] e^{-r^2/\sigma^2(\eta, \omega)} \\ &\times \exp \left\{ i \frac{r^2}{\sigma^2(\eta, \omega)} \frac{\eta}{\eta_0(\omega)} - i\ell\theta - i(2n + \ell + 1) \arctan \left[ \frac{\eta}{\eta_0(\omega)} \right] \right\}, \end{aligned} \quad (7)$$

for arbitrary integer  $n$  and real  $\ell$ , where  $\sigma(\eta, \omega)$  relates to the transversal spot size

$$\sigma(\eta, \omega) = \sigma_0 \sqrt{1 + \eta^2/\eta_0(\omega)^2}, \quad \eta_0(\omega) = \omega \sigma_0^2 \quad (8)$$

and  $f(\omega)$  is an arbitrary function which specifies the frequency spectrum. Notice that the Rayleigh length equivalent  $\eta_0$  differs by a factor of two from the Gaussian beam Rayleigh length  $z_0 = \omega \sigma_0^2/2$ . This is a consequence of the factor of two difference in the first term of Eq. (5). At equal spot sizes  $\sigma_0$ , the Gaussian beams are more confined in the longitudinal direction than the flying focus solutions. Finally,  $L_n^\ell$  are the associated Laguerre polynomials

$$L_0^\ell(x) = 1, \quad (9)$$

$$L_1^\ell(x) = 1 + \ell - x, \quad (10)$$

$$L_n^\ell(x) = \frac{x^{-\ell} e^x}{n!} \frac{d^n}{dx^n} (e^{-x} x^{n+\ell}). \quad (11)$$

Since increasing  $n$  generates higher order polynomials, we can restrict ourselves to the simplest  $n = 0$  case and consider only the  $\ell$ -dependent solution

$$\begin{aligned} \tilde{\mathbf{A}}_{\ell, \perp}(\eta, r, \theta, \omega) &= \mathcal{A}_0 f(\omega) \frac{\sigma_0}{\sigma(\eta, \omega)} \left[ \frac{\sqrt{2}r}{\sigma(\eta, \omega)} \right]^\ell e^{-r^2/\sigma^2(\eta, \omega)} \\ &\times \exp \left\{ i \frac{r^2}{\sigma^2(\eta, \omega)} \frac{\eta}{\eta_0(\omega)} - i\ell\theta - i(\ell + 1) \arctan \left[ \frac{\eta}{\eta_0(\omega)} \right] \right\}. \end{aligned} \quad (12)$$

By substituting this solution back into Eq. (1), we obtain the exact solution of Maxwell's equations

$$\begin{aligned} \mathbf{A}_{\ell, \perp}(\eta, r, \theta, \phi) &= \frac{1}{2} \mathcal{A}_0 \int d\omega f(\omega) e^{-i\omega\phi} \frac{\sigma_0}{\sigma(\eta, \omega)} \left[ \frac{\sqrt{2}r}{\sigma(\eta, \omega)} \right]^\ell e^{-r^2/\sigma^2(\eta, \omega)} \\ &\times \exp \left\{ i \frac{r^2}{\sigma^2(\eta, \omega)} \frac{\eta}{\eta_0(\omega)} - i\ell\theta - i(\ell + 1) \arctan \left[ \frac{\eta}{\eta_0(\omega)} \right] \right\} + \text{c.c.} \end{aligned} \quad (13)$$

This solution allows us to construct spatio-temporally localized pulses of finite energy by tuning the spectral profile  $f(\omega)$ . For example, for the Gaussian frequency profile  $f(\omega) = (\sqrt{\pi}/\tau) \exp[-(\omega - \omega_0)^2 \tau^2]$  and for  $\omega_0 \tau \gg 1$ , we obtain approximately a Gaussian pulse profile proportional to  $\exp(-\phi^2/\tau^2)$  (see [2]). In the limit  $\tau \rightarrow \infty$  the frequency distribution becomes a delta function

$$f(\omega) = \delta(\omega - \omega_0), \quad (14)$$

which describes a simple monochromatic beam solution with infinite extent in both time and space. For this frequency distribution, the integration can be carried out explicitly just by replacing  $\omega \rightarrow \omega_0$

$$\begin{aligned} \mathbf{A}_{\ell, \perp}(\eta, r, \theta, \phi) &= \frac{1}{2} \mathcal{A}_0 \frac{\sigma_0}{\sigma(\eta, \omega_0)} \left[ \frac{\sqrt{2}r}{\sigma(\eta, \omega_0)} \right]^\ell e^{-r^2/\sigma^2(\eta, \omega_0)} \\ &\times \exp \left\{ -i\omega_0\phi + i \frac{r^2}{\sigma^2(\eta, \omega_0)} \frac{\eta}{\eta_0(\omega_0)} - i\ell\theta - i(\ell + 1) \arctan \left[ \frac{\eta}{\eta_0(\omega)} \right] \right\} + \text{c.c.}, \end{aligned} \quad (15)$$

which can be evaluated in terms of real functions as

$$\begin{aligned} \mathbf{A}_{\ell, \perp}(\eta, r, \theta, \phi) &= \mathcal{A}_0 \frac{\sigma_0}{\sigma(\eta, \omega_0)} \left[ \frac{\sqrt{2}r}{\sigma(\eta, \omega_0)} \right]^\ell e^{-r^2/\sigma^2(\eta, \omega_0)} \\ &\times \cos \left\{ \omega_0\phi - \frac{r^2}{\sigma^2(\eta, \omega_0)} \frac{\eta}{\eta_0(\omega_0)} + \ell\theta + (\ell + 1) \arctan \left[ \frac{\eta}{\eta_0(\omega)} \right] \right\}. \end{aligned} \quad (16)$$

From Eq. (2) we have the following expression for  $A_{\ell, -}$

$$A_{\ell, -}(\eta, r, \theta, \phi) = - \int d\phi \nabla_{\perp} \cdot \mathbf{A}_{\ell, \perp}(\eta, r, \theta, \phi). \quad (17)$$

If we assume that the field is linearly polarized along the  $x$ -axis, i.e., for  $\mathcal{A}_0 = \mathcal{A}_0 \hat{x}$ , we can evaluate

$$A_{\ell,-}(\eta, r, \theta, \phi) = -\ell \frac{\mathcal{A}_0}{\omega_0} \frac{1}{r} \frac{\sigma_0}{\sigma(\eta, \omega_0)} \left[ \frac{\sqrt{2}r}{\sigma(\eta, \omega_0)} \right]^\ell e^{-r^2/\sigma^2(\eta, \omega_0)} \sin[\Psi_\ell(1, 0)] \\ + \frac{\mathcal{A}_0}{\omega_0} \frac{x}{\sigma^2(\eta, \omega_0)} \left[ \frac{\sqrt{2}r}{\sigma(\eta, \omega_0)} \right]^\ell e^{-r^2/\sigma^2(\eta, \omega_0)} \sin[\Psi_\ell(0, 1)], \quad (18)$$

where the first term vanishes for  $\ell = 0$ . The phases which appear in the above solution are defined as

$$\Psi_\ell(a, b) = \omega_0 \phi - \frac{r^2}{\sigma^2(\eta, \omega_0)} \frac{\eta}{\eta_0(\omega_0)} + (\ell - a)\theta + (\ell + 1 + b) \arctan \left[ \frac{\eta}{\eta_0(\omega_0)} \right]. \quad (19)$$

Since  $A_{\ell,+} = A_\ell^0 + A_\ell^z = 0$  and  $A_{\ell,-} = A_\ell^0 - A_\ell^z$  we can evaluate the  $A_\ell^0$  and  $A_\ell^z$  components as

$$A_\ell^0 = -A_\ell^z = \frac{1}{2} A_{\ell,-}. \quad (20)$$

Note that for any  $\ell > 1$ , the four-potential on the  $z$ -axis ( $r = 0$ ) vanishes. The case of  $\ell = 1$  is special, because both electric and magnetic fields have only  $z$ -component non-zero on the axis. Thus, in the case of an electron entering such field along the  $z$ -axis, the motion becomes effectively one-dimensional and radiation reaction has very little effect on the electron trajectory (at least according to the Landau-Lifshitz equation).

In the following we will restrict our analysis on  $\ell = 0$  and simplify the notation. For brevity we will denote

$$\sigma(\eta, \omega_0) \rightarrow \sigma_\eta, \quad \eta_0(\omega_0) \rightarrow \eta_0, \quad \Psi_0(0, a) \rightarrow \Psi(a), \quad (21)$$

i.e., we do not indicate explicitly the dependence on  $\omega_0$ , and we drop the index  $\ell = 0$ .

### ELECTRIC AND MAGNETIC FIELDS ( $\ell = 0$ )

The electric and magnetic fields can be calculated from the four-vector potential components as

$$\mathbf{E} = -\nabla A^0 - \frac{\partial \mathbf{A}}{\partial t}, \quad \mathbf{B} = \nabla \times \mathbf{A}, \quad (22)$$

which can be evaluated explicitly knowing the solutions in Eqs. (16) and (18) with  $\ell = 0$ :

$$E_x = \mathcal{A}_0 e^{-r^2/\sigma_\eta^2} (T_1 + T_2), \quad B_x = \frac{2\mathcal{A}_0 xy}{\omega_0 \sigma_0 \sigma_\eta^3} e^{-r^2/\sigma_\eta^2} \sin[\Psi(2)], \quad (23a)$$

$$E_y = \frac{2\mathcal{A}_0 xy}{\omega_0 \sigma_0 \sigma_\eta^3} e^{-r^2/\sigma_\eta^2} \sin[\Psi(2)], \quad B_y = \mathcal{A}_0 e^{-r^2/\sigma_\eta^2} (T_1 - T_2), \quad (23b)$$

$$E_z = \frac{2\mathcal{A}_0 x}{\sigma_\eta^2} e^{-r^2/\sigma_\eta^2} \cos[\Psi(1)], \quad B_z = \frac{2\mathcal{A}_0 y}{\sigma_\eta^2} e^{-r^2/\sigma_\eta^2} \cos[\Psi(1)]. \quad (23c)$$

The two terms  $T_1$  and  $T_2$  are given by

$$T_1 = \frac{\omega_0 \sigma_0}{\sigma_\eta} \sin[\Psi(0)], \quad (24)$$

$$T_2 = -\frac{r^2}{\omega_0 \sigma_0 \sigma_\eta^3} \left\{ \frac{2\sigma_0^2 \eta / \eta_0}{\sigma_\eta^2} \cos[\Psi(0)] + \left( 1 - \frac{2\sigma_0^2 \eta^2 / \eta_0^2}{\sigma_\eta^2} \right) \sin[\Psi(0)] \right\} + \frac{2x^2}{\omega_0 \sigma_0 \sigma_\eta^3} \sin[\Psi(2)]. \quad (25)$$

We can also explicitly construct the field invariants. The invariant  $\mathbf{E} \cdot \mathbf{B}$  is given by

$$\mathbf{E} \cdot \mathbf{B} = \frac{4\mathcal{A}_0^2 \sigma_0^2}{\sigma_\eta^6} xy e^{-2r^2/\sigma_\eta^2} = \frac{2\mathcal{A}_0^2 \sigma_0^2}{\sigma_\eta^6} r^2 \sin(2\theta) e^{-2r^2/\sigma_\eta^2}, \quad (26)$$

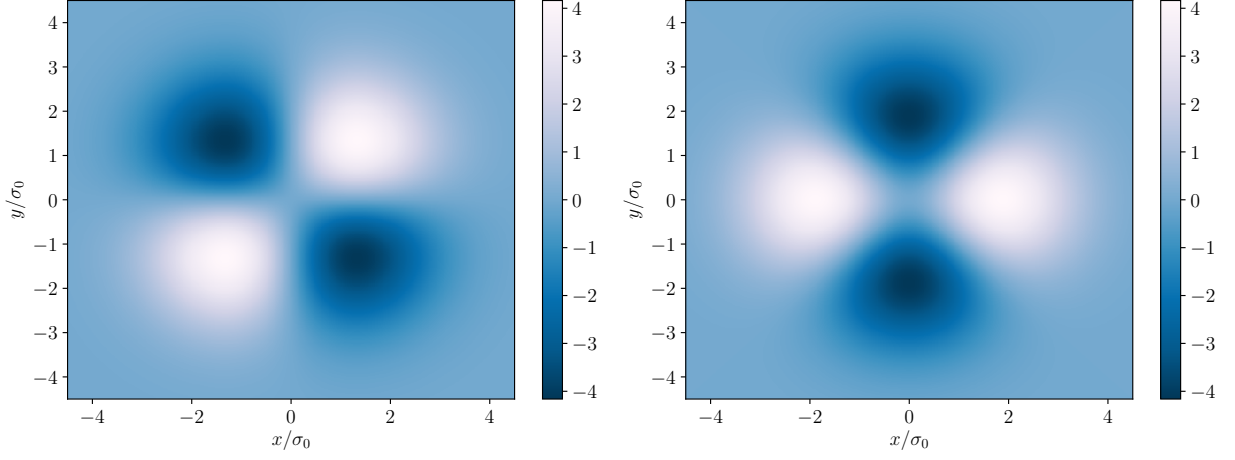


FIG. 1. The invariants  $\mathbf{E} \cdot \mathbf{B}$  (left) and  $(E^2 - B^2)/2$  (right) at the focus ( $\eta = 0$ ) for  $\sigma_0 = 5$  in arbitrary units. The field is polarized along the  $x$ -direction.

which vanishes whenever either  $x$  or  $y$  is zero. Similarly, for the invariant  $(E^2 - B^2)/2$ , we have

$$\frac{1}{2}(E^2 - B^2) = \frac{2\mathcal{A}_0^2\sigma_0^2}{\sigma_\eta^6}(x^2 - y^2)e^{-2r^2/\sigma_\eta^2} = \frac{2\mathcal{A}_0^2\sigma_0^2}{\sigma_\eta^6}r^2 \cos(2\theta)e^{-2r^2/\sigma_\eta^2}, \quad (27)$$

which is zero whenever  $|x| = |y|$ . At the position of the focus  $\eta = 0$  we have  $\sigma(\eta = 0) = \sigma_0$ , and both invariants no longer depend on  $z$  and  $t$ . In Fig. 1 we plot these invariants at focus. Out of the focus  $\eta \neq 0$  for either  $\eta > 0$  or  $\eta < 0$ , both invariants look qualitatively the same as at the focus, and only the spot size  $\sigma_\eta$  increases as the beam defocuses.

### TIME AVERAGES OF THE OSCILLATING FUNCTIONS

The oscillatory parts of the fields obtained above are given by the trigonometric functions of the type

$$\cos[\Psi(a)] = \cos \left[ \omega_0\phi - \frac{r^2}{\sigma_\eta^2} \frac{\eta}{\eta_0} + (1+a) \arctan \left( \frac{\eta}{\eta_0} \right) \right], \quad (28a)$$

$$\sin[\Psi(a)] = \sin \left[ \omega_0\phi - \frac{r^2}{\sigma_\eta^2} \frac{\eta}{\eta_0} + (1+a) \arctan \left( \frac{\eta}{\eta_0} \right) \right]. \quad (28b)$$

We want to examine how products of these functions behave at some fixed  $z$  and perform the time average under the assumption that the oscillations in  $\phi$  are much faster than how fast the intensity envelope in  $\eta$  varies, i.e.,  $\sigma_0^2 \gg \lambda_0^2/\pi$ . By using the angle addition formulas and the averages

$$\langle \cos^2(\omega_0\phi) \rangle_z = \frac{1}{2}, \quad \langle \sin^2(\omega_0\phi) \rangle_z = \frac{1}{2}, \quad \langle \sin(\omega_0\phi) \cos(\omega_0\phi) \rangle_z = 0, \quad (29)$$

over time at some fixed  $z$ , the time-averages of the products of interest then become

$$\langle \sin[\Psi(a)] \cos[\Psi(b)] \rangle_z = \frac{1}{2} \sin \left[ (a-b) \arctan \left( \frac{\eta}{\eta_0} \right) \right], \quad (30a)$$

$$\langle \sin[\Psi(a)] \sin[\Psi(b)] \rangle_z = \frac{1}{2} \cos \left[ (a-b) \arctan \left( \frac{\eta}{\eta_0} \right) \right], \quad (30b)$$

$$\langle \cos[\Psi(a)] \cos[\Psi(b)] \rangle_z = \frac{1}{2} \cos \left[ (a-b) \arctan \left( \frac{\eta}{\eta_0} \right) \right]. \quad (30c)$$

As it is clear from these expressions, the slowly-varying time dependence in  $\eta = t + z$  is still kept. Note that the final formulas can be evaluated in terms of  $\sigma_\eta$ ,  $\sigma_0$ ,  $\eta$ ,  $\eta_0$  as

$$\sin \left[ \arctan \left( \frac{\eta}{\eta_0} \right) \right] = \frac{\sigma_0 \eta / \eta_0}{\sigma_\eta}, \quad \cos \left[ \arctan \left( \frac{\eta}{\eta_0} \right) \right] = \frac{\sigma_0}{\sigma_\eta}, \quad (31a)$$

$$\sin \left[ 2 \arctan \left( \frac{\eta}{\eta_0} \right) \right] = 2 \frac{\sigma_0^2 \eta}{\sigma_\eta^2 \eta_0}, \quad \cos \left[ 2 \arctan \left( \frac{\eta}{\eta_0} \right) \right] = \frac{\sigma_0^2}{\sigma_\eta^2} \left( 1 - \frac{\eta^2}{\eta_0^2} \right), \quad (31b)$$

which can be continued for higher  $(a - b)$  values using the angle addition formulas.

### POWER IN THE FLYING FOCUS BEAM

The average power flowing through the  $xy$  plane at a given  $z$  can be calculated as the Poynting vector flux

$$P_{\text{ave}} = \int dx dy \langle \mathbf{E} \times \mathbf{B} \rangle_z \cdot \hat{\mathbf{z}}, \quad (32)$$

where  $\hat{\mathbf{z}}$  is the unit vector normal to the  $xy$  plane, i.e.,  $\hat{\mathbf{z}} = (0, 0, 1)$ . Therefore, we need to evaluate the quantity

$$P_{\text{ave}} = \int dx dy \langle E_x B_y - E_y B_x \rangle_z. \quad (33)$$

The second term is easily computed as

$$\int dx dy \langle E_y B_x \rangle_z = \int dx dy \frac{4\mathcal{A}_0^2 x^2 y^2}{\omega_0^2 \sigma_0^2 \sigma_\eta^6} e^{-2r^2/\sigma_\eta^2} \langle \sin^2[\Psi(2)] \rangle_z = \frac{\pi}{16\omega_0^2 \sigma_0^2} \mathcal{A}_0^2. \quad (34)$$

The first term reads

$$\int dx dy \langle E_x B_y \rangle_z = \int dx dy \mathcal{A}_0^2 e^{-2r^2/\sigma_\eta^2} \langle T_1^2 - T_2^2 \rangle_z. \quad (35)$$

The first part of this expression proportional to  $T_1^2$  can be again directly evaluated, and the result is

$$\int dx dy \mathcal{A}_0^2 e^{-2r^2/\sigma_\eta^2} \langle T_1^2 \rangle_z = \int dx dy \mathcal{A}_0^2 e^{-2r^2/\sigma_\eta^2} \frac{\omega_0^2 \sigma_0^2}{\sigma_\eta^2} \langle \sin^2[\Psi(0)] \rangle_z = \frac{\pi}{4} \mathcal{A}_0^2 \omega_0^2 \sigma_0^2. \quad (36)$$

Finally, the last term is given by

$$\int dx dy \mathcal{A}_0^2 e^{-2r^2/\sigma_\eta^2} \langle T_2^2 \rangle_z \quad (37)$$

and we need to evaluate the square and the time average of the expression (25). After some algebraic manipulations and using the formulas (30a-30c) for the time averages, we obtain

$$\langle T_2^2 \rangle_z = \frac{2}{\omega_0^2 \sigma_\eta^6 \sigma_0^2} (r^4/4 + x^4 - r^2 x^2). \quad (38)$$

Now, we can integrate this expression over the transversal plane:

$$\int \mathcal{A}_0^2 e^{-2r^2/\sigma_\eta^2} \langle T_2^2 \rangle_z dx dy = \frac{\pi}{16\omega_0^2 \sigma_0^2} \mathcal{A}_0^2. \quad (39)$$

We see that in all of the integrals above the dependence on  $\eta$  drops out, as one would expect, and the result is constant and finite. Altogether for the power we have

$$P_{\text{ave}} = \frac{\pi}{4} \mathcal{A}_0^2 \left( \omega_0^2 \sigma_0^2 - \frac{1}{2\omega_0^2 \sigma_0^2} \right) \approx \frac{\pi}{4} \mathcal{A}_0^2 \omega_0^2 \sigma_0^2 \doteq 21.5[\text{GW}] \left( \xi_0 \frac{\sigma_0}{\lambda_0} \right)^2, \quad (40)$$

where  $\xi_0 = |e|\mathcal{A}_0/m$  is the dimensionless normalized field amplitude. Consistently with our approximations, the second term in Eq. (40) can be neglected. In fact, already for  $\sigma_0 = \lambda_0$  the error resulting from omitting this term is  $\approx 0.03\%$ . The full expression shows that with decreasing  $\sigma_0$ , the power decreases until it would vanish at  $\sigma_0/\lambda_0 = 2^{-5/4}\pi^{-1} \approx 0.14$ . However, for such small value of  $\sigma_0$ , our assumption that the field is oscillating much faster than the envelope no longer applies, and the result for the average beam power is not valid. Finally, we would like to point out that the resulting expression is the same as the equivalent expression for the Gaussian beams, with  $\sigma_0$  being the spot size at focus (see for example [4, 5]).

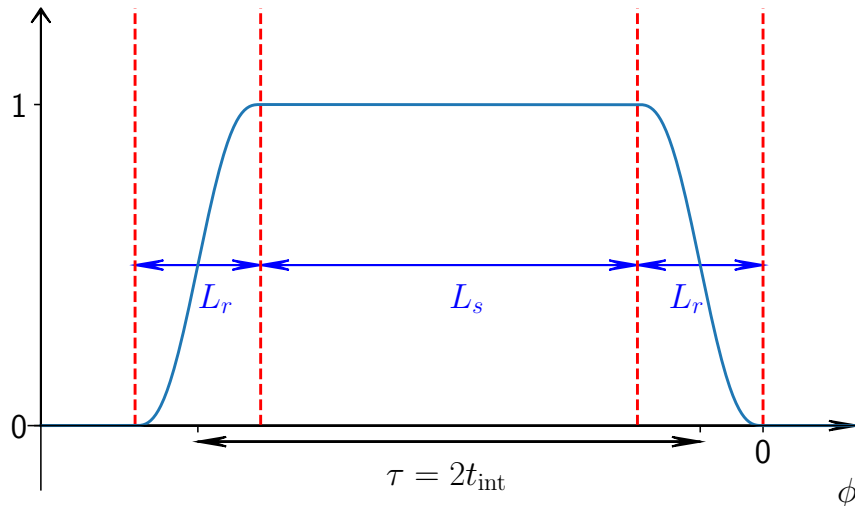


FIG. 2. The  $g(\phi)$  pulse envelope function.  $L_r$  is the length of the ramps and  $L_s$  the length of the flattop region.

### PULSE ENVELOPE

As we described in the Letter we implemented the pulse envelope  $g(\phi)$  on the level of a multiplicative factor modifying the fields (23a-23c). In doing so, the fields no longer satisfy the Maxwell equations exactly, but as long as the derivatives of the function  $g(\phi)$  are small compared to the derivatives of the fields itself, the error is not large and is confined to ramp on/off regions. The functional prescription of the function  $g(\phi)$  is given by 5th order polynomials ensuring smooth transition between the regions where  $g(\phi) = 0$  and  $g(\phi) = 1$  including the first derivatives. Specifically, we have

$$g(\phi) = \begin{cases} -10 \left(\frac{\phi}{L_r}\right)^3 - 15 \left(\frac{\phi}{L_r}\right)^4 - 6 \left(\frac{\phi}{L_r}\right)^5 & -L_r < \phi \leq 0, \\ 1 & -L_r - L_s < \phi \leq -L_r, \\ 10 \left(\frac{\phi+2L_r+L_s}{L_r}\right)^3 - 15 \left(\frac{\phi+2L_r+L_s}{L_r}\right)^4 + 6 \left(\frac{\phi+2L_r+L_s}{L_r}\right)^5 & -2L_r - L_s \leq \phi \leq -L_r - L_s, \\ 0 & \text{otherwise,} \end{cases} \quad (41)$$

where  $L_r$  indicates the length of the ramps and  $L_s$  is the length of the flattop region. We set the length of the pulse  $\tau$  to be equal to  $\tau = L_s + L_r$  to minimize the effect of the ramps. See Fig. 2 for illustration. The whole pulse envelope can be also displaced by replacing  $\phi \rightarrow \phi + \phi_0$  ensuring the correct timing of the electron interaction with Gaussian, respective flying focus pulses. Finally, we choose the length of the ramp  $L_r = 40 \text{ } 1/k_0$  consistently for all simulations. This length is arbitrary as long as it is not too short (to violate the slowly changing pulse envelope approximation) or too long (to significantly affect the pulse length). We also convinced ourselves that our numerical results are robust with respect to variations in  $L_r$ .

- 
- [1] E. Esarey, P. Sprangle, M. Pilloff, and J. Krall, *J. Opt. Soc. Am. B* **12**, 1695 (1995).
  - [2] A. Di Piazza, *Phys. Rev. A* **103**, 012215 (2021).
  - [3] A. Siegman, *Lasers* (University Science Books, 1986).
  - [4] E. Esarey, S. K. Ride, and P. Sprangle, *Phys. Rev. E* **48**, 3003 (1993).
  - [5] Y. I. Salamin, *Appl. Phys. B* **86**, 319 (2007).